

ALICE/INT-2002-19
Internal Note/DIM
May 14, 2002

The RELCAM, an optical transparent sensor for geometry alignment and monitoring systems

J.Y. Grossiord, G. Jacquet

*Institut de Physique Nucléaire de Lyon
IN2P3-CNRS et Université Claude Bernard, Lyon-I
43 Bd du 11 novembre 1918, 69622 Villeurbanne, France*

Yu. Margaryan

*Yerevan Physics Institute
Br. Alikhanian st. 2, 375036 Yerevan, Armenia*

Abstract

The RELCAM (for REflected Light CAmera Monitor), a new transparent photosensor is described. It is based on the reflected light picture monitored by a miniature video-camera with CMOS IC pixel photosensor. Prototype investigations show that an intrinsic r.m.s. value of $\sigma_{res.} = 0.5 \mu\text{m}$ (resolution FWHM = $1.2 \mu\text{m}$), and a stability better than $0.8 \mu\text{m}$ per $^{\circ}\text{C}$ in temperature can be achieved. The linearity function over the full active surface of the sensor has been measured, and method for its correction is proposed.

1 Introduction

The development of transparent photosensors has acquired a real extend due to their possible application in "Slow Control" system for alignment and monitoring of detectors in large High Energy Physics experiments. Currently, a few types of such sensors are developed for ATLAS, CMS, and ALICE experiments at CERN and provide a good (few microns) position resolution. Some of them use a laser beam as reference. For example the ALMY sensor [2, 3] uses IR light transparent micro-strip silicon detector. The STAMP sensor [4] is based on CCD cameras detecting the reflective laser light from two glass splitters. The RELMY sensor uses reflected light detection by quadrant photodiodes [5]. Some others are pure optical systems. We must quote the RASNIK device [6], consisting of an image source, a focusing lens, and an image sensor. Several systems, more or less complex, have been developped starting from that original idea.

This type of photosensors are intent to be applied in multipoint geometry monitoring systems. Therefore, they have to provide several requirements such as a high position resolution (of the order of the micron) and a good linearity, a good stability during a long time scale, a high transmittance, a high radiation tolerance, a simple construction, a low cost, ...

In this paper the RELCAM (REflected Light CAmera Monitor), a new transparent sensor is described. Its performances are presented. It should be an appropriate device to be used for the monitoring system of the ALICE dimuon forward spectrometer [7].

2 The RELCAM sensor

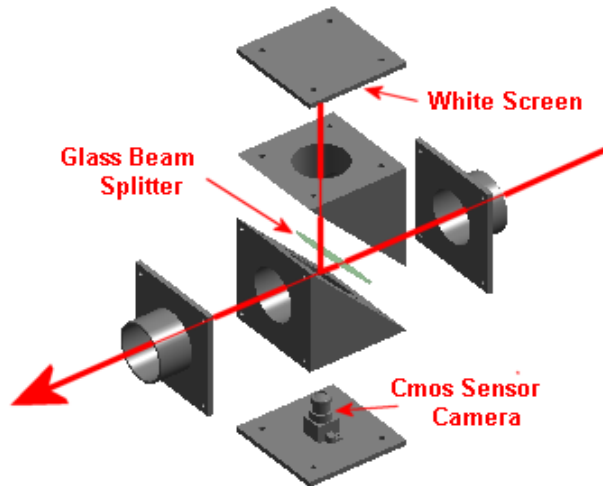


Figure 1: Schematic design of the RELCAM sensor.

A schematic view of the RELCAM sensor is shown in Fig. 1. A semi-transparent mirror, inclined at 45 degrees relatively to the beam direction, reflects less than 10% of the light on a white screen where the picture of the spot is formed. Several materials ($2\text{ }\mu\text{m}$ pelicle film, $3\text{ }\mu\text{m}$ mylar film, 0.5 and 1 mm glass plates) can be used for the reflection. The present tests have been carried out using a 0.5 mm thick glass plate with an anti-reflective coating of its side opposite to the laser beam entrance within the wavelength range of 600-800 nm. An increase up to 95% of the transmittance and the suppression of the interference of light spots reflected from both surfaces can be achieved.

The light spot is monitored by a miniature camera of $17 \times 17 \times 30\text{ mm}^3$ in dimension, including the lens. This single ship monochrome camera is equipped with a CMOS 1/3 inch sensor composed of 628×582 pixels, covering a surface of $5.78 \times 4.19\text{ mm}^2$. The sensor has a dynamics range greater than 72 db, a signal/noise ratio greater than 48 db, a sensitivity smaller than 0.5 lux. It provides an efficient spectral response centered at 785 nm which corresponds to the laser beam source wave length. The photo-objective of the camera (focal length of about 8 mm) focuses the light spot from the screen on the pixel matrix. The distance between the screen and the camera is chosen in such a way that a square of $2 \times 2\text{ cm}^2$ on the screen is included within the pixel matrix surface. All parts of RELCAM are assembled in an aluminium box of $70 \times 70 \times 80\text{ mm}^3$ in volume.

3 The RELCAM characteristics

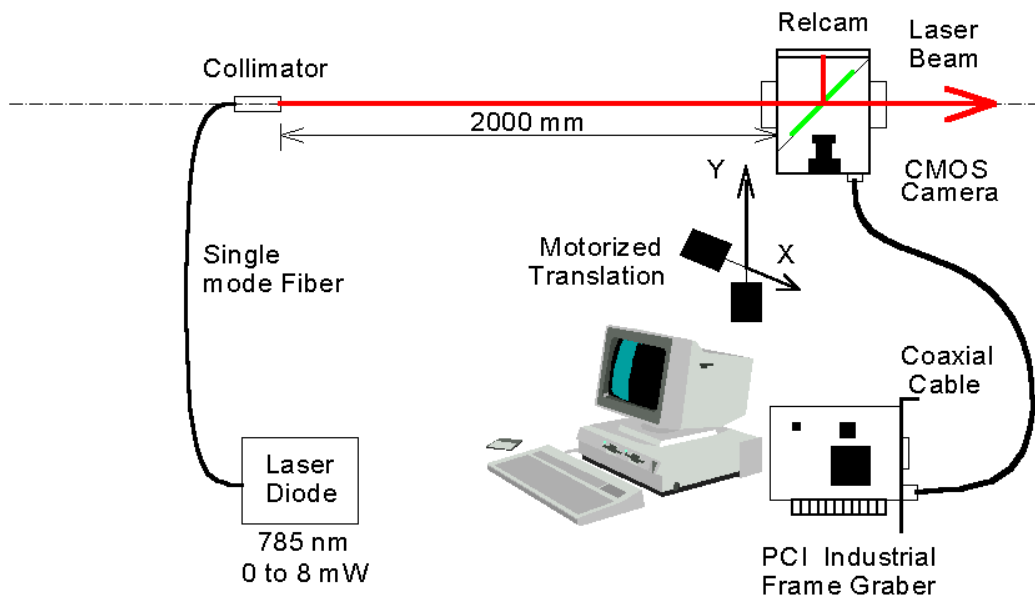


Figure 2: Test bench for the RELCAM sensor.

A test bench based on a granit table of $2.5 \times 0.5 \text{ m}^2$ in surface has been used for measurements of the RELCAM characteristics (Fig. 2). The beam source consists of a 785 nm laser diode (type 61FCM from "Schafter and Kirchhoff") coupled with a single-mode fibre. It provides a circular beam cone. Its intensity distribution is Gaussian and has a small coherence length to reduce the speckle contrast. At the end of the single mode fibre, a focusable collimator is used to obtain a beam with a median diameter of 4.5 mm at 10 m and a divergence of 0.12 mrd. The RELCAM sensor provides a video signal which is digitized by an industrial frame grabber in an 8-bit (per pixel) matrix and then transferred (in units of four pixels, corresponding to 32-bit words) to the memory of a computer. It is mounted on two-axis motorized translation stages with 100 mm excursion ranges. Their resolution in position is $0.5 \mu\text{m}$ with a reproducibility of $1.5 \mu\text{m}$. The scan movements and the data acquisition are controlled by a computer.

The laser beam spot distribution as recorded by the system is shown in Fig. 3. In that figure, the x and y horizontal values are expressed in pixels of the video monitor. 768 video pixels correspond to 5.78 mm (628 CMOS pixels) and 576 video pixels to 4.19 mm (582 CMOS pixels). A simple analysis of the picture is obtained by thresholding the amplitude (to eliminate the residual noise on the whole surface of the sensor) and summing the pixel signals in the x and y directions. The corresponding beam coordinates are given by the centers of gravity of the x and y distributions.

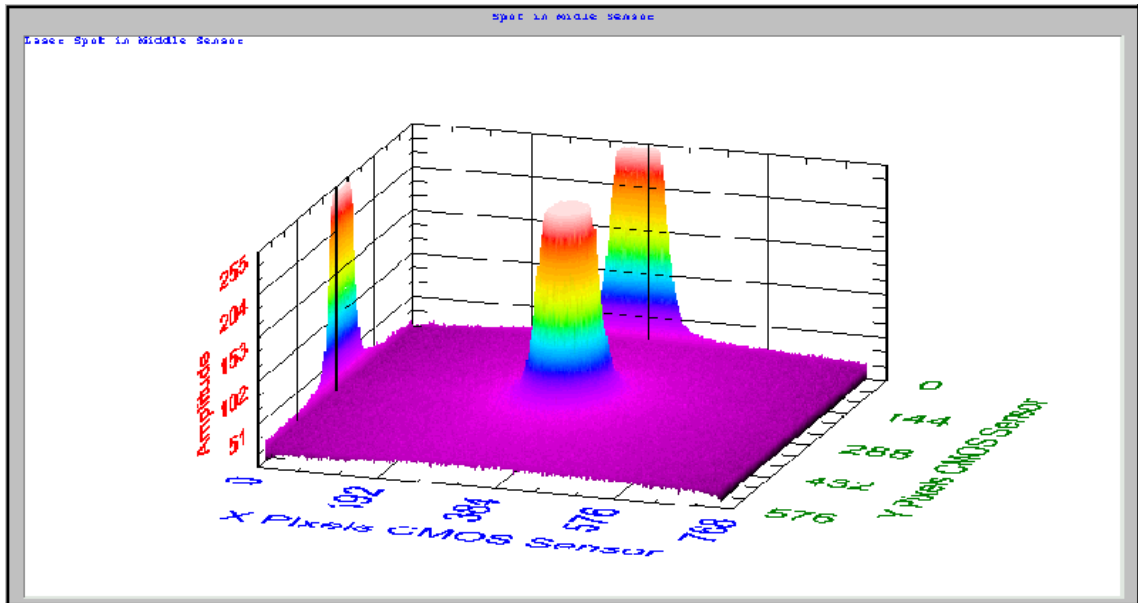


Figure 3: The laser beam spot distribution.

3.1 Resolution

Measurements of laser beam center of gravity distributions, as shown in Fig. 3, have been obtained for three positions of the beam near the optical axis of the camera and at interval of $10\text{ }\mu\text{m}$ along the x direction. At each position, 500 measurements are carried out. The projection of the spots on the x direction is shown in Fig. 4a. The calibration of the sensor in the central part of its aperture ($x = x_0 \approx 0$) can thus be extracted. About .35 video pixel represents a $20\text{ }\mu\text{m}$ displacement, which gives about $56.5\text{ }\mu\text{m}/\text{pixel}$. A r.m.s. value $\sigma_{res.} = 0.5\text{ }\mu\text{m}$ is measured, which corresponds to a full width at half maximum (FWHM) of $1.2\text{ }\mu\text{m}$ (Fig. 4b). This procedure repeated in the y direction leads to a calibration coefficient of $60.3\text{ }\mu\text{m}/\text{pixel}$ and similar r.m.s and FWHM values.

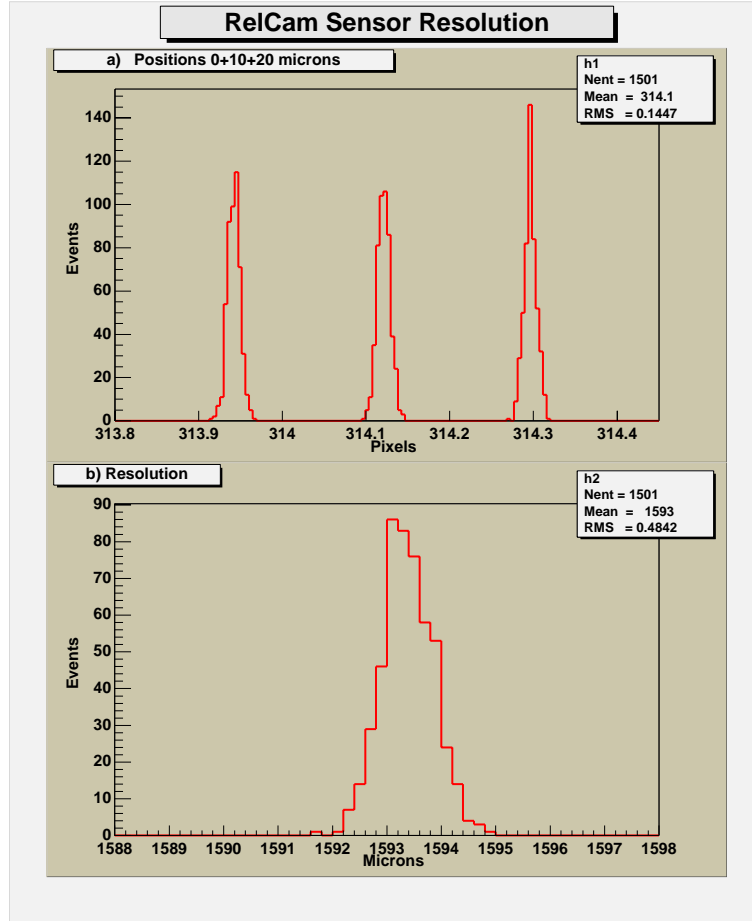


Figure 4: Three laser spots projected on the x direction of the pixel sensor.

The calibration of this type of sensors around the center of its optical covering is a main requirement. It is the nominal calibration. The evolution of these calibration parameters with the distance relative to the center of the aperture is presented in Section 3.3.

3.2 Stability

One of the most important specifications of sensors is their stability during the time. In order to evaluate this characteristics, a sensor was directly set on the granit table at 12 cm from the beam collimator so that the influence of several external factors (air condition, angular instability of the beam, thermal expansion of the supports, ...) are minimized. The position of the laser beam has been measured periodically during 90 hours. The results are given in Fig. 5. It gives the variation of the room temperature as a function of the time and the stability of the x and y positions of the laser beam during the exposure. We observe a clear correlation between the measured coordinates and the room temperature. Room temperature has changed during this time from 16°C to 19.5°C. As it is seen in Fig. 5, maximum variations of the x and y coordinates are about 2 μm and 2.5 μm respectively. An effect lower than 0.75 μm per °C (0.57/0.71 μm per °C in the x/y direction) is thus recorded as the maximum shifting value of the beam spot position in both directions. It has to be noticed that these numbers represent a global effect due to the several elements of the sensor, including the camera and its housing.

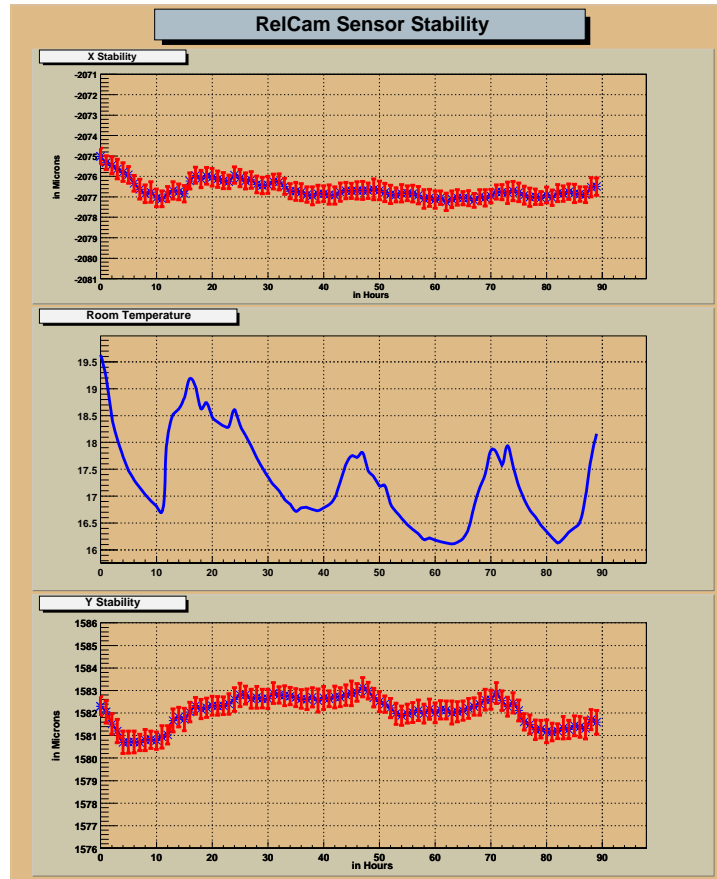


Figure 5: x , y laser beam spot positions and room temperature as a function of the time.

3.3 Linearity

A first linearity measurement at $x = 0$ in the y direction has been carried out. The result is shown in Fig. 6. As expected, $60.3 \mu\text{m}/\text{pixel}$ are recorded with a good first order linearity through the scanned 17 mm interval.

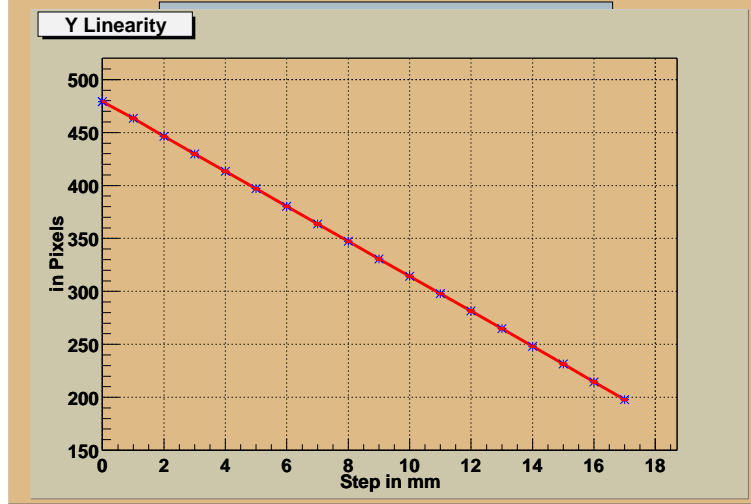


Figure 6: Linearity of the sensor in the y direction.

Then, the full surface of the pixel matrix of the camera has been scanned as followed. The spot of the partially reflected light of the laser beam is moved on the $20 \times 20 \text{ mm}^2$ flat screen area of the sensor by steps of 1 mm in the two directions. At each position, the x and y centers of gravity of the spot are calculated with the nominal calibration values as defined Section 3.1. The difference between the measured coordinates $\rho = \sqrt{(x^2 + y^2)}$ and the coordinates given by the translation stages $\rho_0 = \sqrt{(x_0^2 + y_0^2)}$, namely the residual, is calculated as a function of x_0 and y_0 . The results are shown in Fig. 7. A spherical surface which contains the $x_0 = 0$ and $y_0 = 0$ bin shows clearly the linearity function of the system in the two directions. A difference of about $240 \mu\text{m}$ ($\sigma_\rho = 44 \mu\text{m}$) is measured from the center to the edge of the matrix. This no flat surface is due to the optical aberrations provided by the lens system of the camera. Larger the distance of the optics center, larger the distortion.

In a second stage of the study, we have tried to eliminate these aberration effects by just giving a spherical shape to the screen. A 10 cm radius spherical surface has been shaped before repeating the scan as described above. The results are given in Fig. 8. It shows a very efficient correction of the aberrations with a residual range reduced to about $70 \mu\text{m}$ ($\sigma_\rho = 14 \mu\text{m}$). Nevertheless, this correction method suffers two limitations. The first is the difficulty for a precise determination of the screen radius for a total compensation. The second is the impossibility to perfectly superpose the spherical screen axis and the

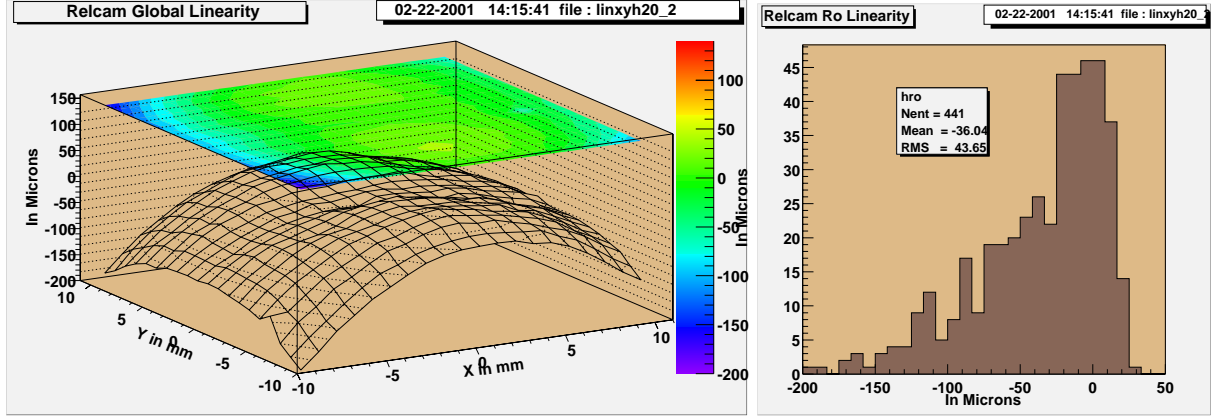


Figure 7: Residual $\sqrt{(x^2 + y^2)} - \sqrt{(x_0^2 + y_0^2)}$ given by the RELCAM sensor with a flat screen as a function of x_0 and y_0 (left) and integrated on all the x_0 and y_0 values (right).

optical axis of the camera. We have to correct geometrical effects well beyond what the usual mechanics precision can provide.

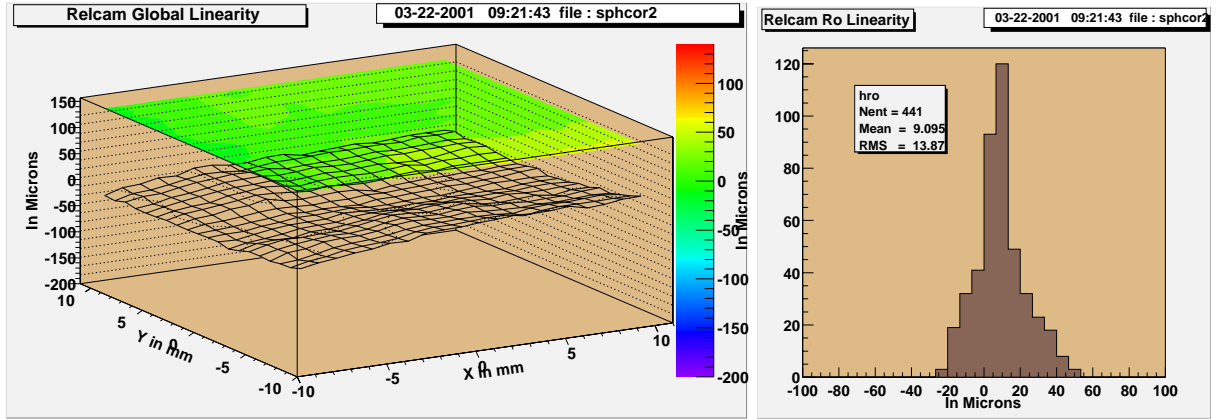


Figure 8: Residual $\sqrt{(x^2 + y^2)} - \sqrt{(x_0^2 + y_0^2)}$ given by the RELCAM sensor with a spherical screen as a function of x_0 and y_0 (left) and integrated on all the x_0 and y_0 values (right).

In order to bypass this difficulty, we propose, instead of shaping the screen, a software correction. More specifically, the sensor can be associated to two correction files, the first one for correction along the x direction, the second one for correction along the y direction. The correction of the x measurement is the residual values $x - x_0$ at each x_0 and y_0 positions, positions given by the moving stages. Fig. 9 shows the residual $x - x_0$ plotted as a function of x_0 and y_0 and the distribution of their values which are all included within $180 \mu\text{m}$ ($\sigma_x = 39 \mu\text{m}$).

In practice, each measure of x with the sensor (and its nominal calibration) can be corrected from distortion effects by the $x - x_0$ residual, value taken at $x_0 = x$ and $y_0 = y$. We have verified that such a procedure leads to suppress the non linearity effects and

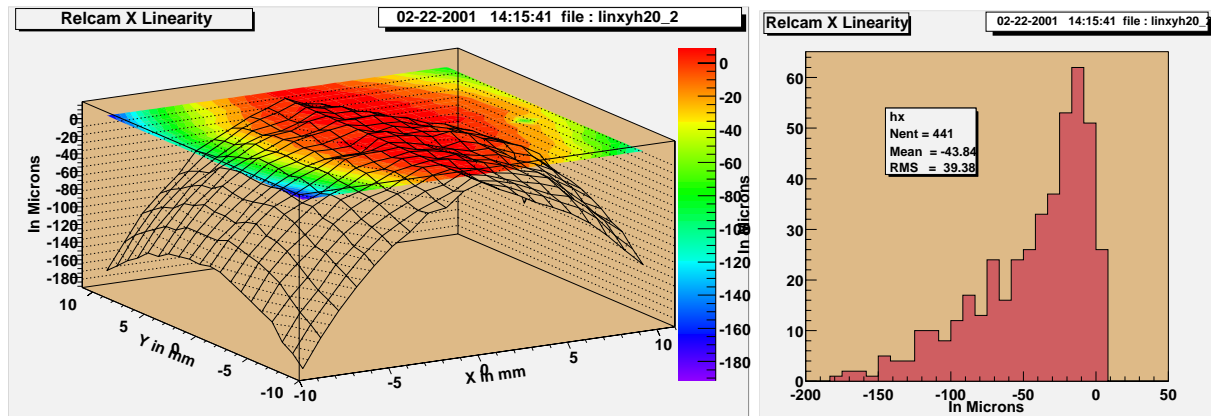


Figure 9: Residual $x - x_0$ given by the RELCAM sensor with a flat screen as a function of x_0 and y_0 (left) and integrated on all the x_0 and y_0 values (right).

to recover the nominal resolution of the sensor ($\sigma_{res.} = 0.5 \mu\text{m}$) through the full surface of the pixel matrix. A similar procedure can be repeated to calculate the corrected y coordinate. In this case, the $y - y_0$ residual values taken at $x_0 = x$ and $y_0 = y$ are used.

4 Conclusion

We have developped a new transparent photosensor based on a video camera. The semi-reflected light from laser beam forms a spot on a screen which is continuously recorded by the camera. The performances of the system within a $20 \times 20 \text{ mm}^2$ surface range can be summarized as followed:

- intrinsic resolution of about $\sigma_{res} = 0.5 \mu\text{m}$ (FWHM = $1.2 \mu\text{m}$),
- stability with the temperature better than $0.75 \mu\text{m}$ per $^\circ\text{C}$,
- raw linearity in the full plane of excursion within $240 \mu\text{m}$ ($\sigma = 44 \mu\text{m}$),
- no-linearity effects suppressed through software corrections.

The tests of the sensor will be pursued so that the effects of the laser beam focalisation and power on its performances can be quantified. Moreover, magnetic field and radiation effects will be evaluated.

Acknowledgements

The work is supported by INTAS project 99 CERN - 0118. One of us (Y.M.) spent three months at IPN-Lyon thanks to a grant allocated by the IN2P3-CNRS. We would like to thank A. Grigoryan for fruitful discussions and C. Combaret for his help during the use of the data acquisition system.

References

- [1] W. Blum et al., Nucl. Instr. and Meth. in Phys. Res., A377(1996)404.
- [2] M.Fernandez Garcia et al., Nucl. Instr. and Meth. in Phys.Res., A461(2001)213.
- [3] F.Bauer et al., IEEE Transactions on Nuclear Science (June issue), MPI report, MPI-PhE/2000-30, October 2000.
- [4] J.-Ch. Bariere et al., <http://www.dapnia.cea.fr/Doc/Publications/Archives/99-04>.
- [5] V. D. Danielyan et al., ALICE/99-27, Internal Note/DIM (1999).
- [6] P. Duinker et al., Nucl. Instr. and Meth. in Phys. Res., A273(1988)814.
- [7] Dimuon Forward Spectrometer, Technical Design Report, CERN/LHCC 99-22, ALICE TDR 5, 13 August 1999; CERN/LHCC 2000-046, Addendum 1 to ALICE TDR 5, 15 December 2000.